Uncertainty in Acoustical Modeling

Sheri L. Martinelli, D. Keith Wilson, Andrew S. Wixom, and Chris L. Pettit

Introduction

In acoustics, as in many fields, complex phenomena are often described with representations, or *models*. Unfortunately, all models are inherently imperfect representations of the real world. As the mathematician von Neumann (1947, p. 626) put it, "Truth is much too complicated to allow anything but approximations." Often, the models are highly idealized; for example, a fish may be represented as a cylinder in an acoustical scattering calculation. Similarly, a room may become a rectangular box and the ocean a homogeneous layer of water bounded above by air and below by sediment. Such simplifications can provide invaluable insights into acoustical phenomena, however. These idealizations allow us to express mathematically how sound waves interact with a fish, a room, or the ocean. The error incurred in making these approximations is called *model error* and is one component of the *error budget* (Pettit and Wilson, 2017) that all modeling efforts seek to balance against model fidelity.

Computers make it possible to create much more realistic models by translating the mathematical equations into computer code that can perform many more calculations than a mathematician can with a pencil. Increasing model fidelity (adding complexity to create a more detailed representation) can greatly reduce the model error. For example, the fish can have fins and a tail, the room can have balconies and seats, and the ocean can have a wavy surface and rocks in the sediment. The important acoustical effects arising from these examples would be intractable without computers. However, a computational model differs in important ways from a mathematical model. The mathematical model uses assumptions to simplify the physics. To solve the equations on a computer, they must be *discretized* for representation on a finite precision machine. For instance, integrals become weighted sums and derivatives become finite differences; this introduces error into the computational model that is not present in the mathematics. A second component of the error budget is the *discretization error*. It can be reduced by operations such as grid refinement or more advanced numerical methods.

Because models, whether computational or analytical, have these inherent errors due to simplifications, laboratory and field experiments remain essential for validating models and understanding acoustical phenomena. Real-world data are also needed as the model's input. Any data used to inform the model will have errors due to sensor calibration, resolution, and natural variability of the quantity being measured. This *measurement error* is another term in the error budget. For example, it is impossible to measure every grain of sand for input to an ocean acoustics model, and the action of taking a core sample disturbs the layered structure of the sediment, making any future description of this variable incorrect.

This article focuses on the final piece of the error budget, one that is perhaps the least often considered, *statistical error*. Indeed, most computational acoustics models are still constructed from a *deterministic* perspective, meaning that all parameters required to solve the mathematical expressions are specified as though exactly known. In contrast, experimentalists are usually aware that, even in highly controlled laboratory environments, measurement errors are always present and introduce *uncertainty* into observations, which must be captured by a suitable error analysis.

It is similarly important in computational modeling to assess how uncertainties in model inputs affect the outputs. An ocean acoustic propagation model, for example, needs information about seabed composition to compute the sound field in the water. But the seabed composition cannot be measured everywhere, and the measurements themselves are subject to error. Thus, the sediment properties can only be represented probabilistically. This, in turn, affects how much sound is reflected from and transmitted into the seabed. Characterizing the probability distribution of the output, in this case the sound field, is

 https://doi.org/10.1121/AT.2023.19.2.28

not necessarily straightforward. A common assumption is that each source of error is independent, and the uncertainty retains the same form in the model output. But this is inappropriate when the output depends on many complex nonlinear interactions. Misapplication of statistical information or failure to take uncertainty into account can undermine the utility and perception of the model itself.

To fully address the impact of uncertainties on the model output, modelers adopt the *probabilistic* perspective (**Figure 1**). The model is still a representation of a physical system, which relates a number of input parameters to an output quantity of interest (QoI). However, in the probabilistic perspective, *probability distributions* (which measure the likelihood that a variable takes on a particular value or range of values) are used to represent uncertainties in the parameters and QoI. Weather forecasting provides a familiar example. Forecast models are typically initialized with satellite and weather balloon data, which by nature imperfectly characterize the exact state of the atmosphere. The models then predict a QoI such as the path of a hurricane, as conveyed by the "cone of uncertainty" on the weather map used by emergency management agencies and the public to prepare for storms.

Considerations in Computational Modeling

Modelers use *uncertainty* in the general sense of a lack of knowledge. Uncertainties can be decomposed into two broad types, *epistemic* and *aleatory*. Epistemic uncertainty arises from *imperfect knowledge* of the parameter. Aleatory uncertainty is caused by actual *random variability*, for example, whether a coin toss lands on heads or tails. However, categorizing the types of uncertainty can be challenging because most practical uncertainties have elements of both types. For example, human or animal behaviors exhibit random variability because understanding of all factors driving such behaviors is extremely limited. As more is learned about biological drivers of behavior, uncertainty can be reduced (epistemic), but variables like the subject's motivation are necessarily aleatory. However, regardless of the type of uncertainty, they can be treated the same way mathematically, with probability distributions. For a more thorough discussion of the types of uncertainty, among other related definitions and techniques, see Smith (2013).

Figure 1. *Probabilistic perspective on modeling. The model is a mathematical or computational representation of a physical system. It relates a number of input parameters to an output quantity of interest (QoI). In the probabilistic perspective, the parameters and QoI are described by probability distributions.*

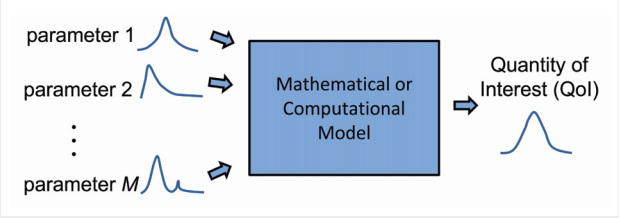

In this article, we focus on uncertainty describable with random variables or processes. For example, the location of an acoustic source in an experiment may be unknown and represented by a random variable that is uniformly distributed over some region. The size of the region could be reduced with more accurate measurement techniques (thus exemplifying epistemic uncertainty), whereas measurement errors that can be described only in probabilistic terms would be aleatory.

Computational techniques for incorporating uncertainty into a model can be classified into two types: intrusive and nonintrusive. An intrusive method's mathematical formulation changes the underlying model and thus requires reworking a computer program. Because a great deal of effort and resources go into developing and testing deterministic computer codes, we focus here on nonintrusive methods, which permit reuse of existing programs. For example, suppose a colleague has provided a complex code for calculating the reverberation time of a room given its dimensions and construction materials. Incorporating uncertainty, perhaps in the absorption coefficient of the wall paneling, in an intrusive manner would require modifying that code to handle the details of the uncertainty directly. However, a nonintrusive technique employs the code in a "black box" sense, only needing to evaluate the reverberation time using the existing code at certain values of its inputs.

Among nonintrusive methods, Monte Carlo simulation (MCS) is the most widely known. However, more recently, generalized polynomial chaos (GPC) expansions have gained ground as both an alternative and a complementary approach to MCS. GPC can be more efficient than MCS for certain problems and produces a stochastic representation of a computational expensive code, called a *metamodel*. And, importantly, in practice the metamodel

is generally much less computationally expensive in terms of CPU time and memory to evaluate than the original code. Data-based approaches (e.g., Gaussian process regressions) can be combined with these methods to bridge the gap between equation-based models and experimental data. In this article, we discuss the MCS and GPC approaches and demonstrate their application using a classical problem in acoustics, namely the Lloyd's mirror, which, despite its relative simplicity, richly illustrates the hazards of neglecting uncertainties and how probabilistic approaches can address this problem.

What Is the Lloyd's Mirror Effect?

The Lloyd's mirror effect (named after Humphrey Lloyd, 1800-1881) is the pattern of constructive and destructive interference occurring when sound waves encounter a flat, reflective boundary. A previous article in *Acoustics Today* (Carey, 2009) described this effect and its history in detail. Although Carey's article focused on Lloyd's mirror in the context of underwater acoustics, it occurs in many other situations, such as in the atmosphere above the ground and indoors next to a wall. The geometry is illustrated in **Figure 2**. We have adopted the coordinate convention typical of atmospheric acoustics, with the vertical axis upward.

Although there is only one physical acoustic source in the Lloyd's mirror problem (the jet), the presence of the reflective boundary surface creates a pressure field consisting of the sum of two *apparent* sources, one representing sound from the actual source and the other from a so-called *image* source. The image source is located an equal distance from the true source on the other side of the reflecting boundary (**Figure 2**). In the present work, we assume a perfectly *rigid* boundary that occurs for propagation in air above a denser, harder medium such as water or rock. In this case, the image source is equal in magnitude and phase to the true source. However, if the reflecting surface has a different shape (such as a dome or wavy ocean surface), or different material properties (such as sound absorbing material), then the relationship between the source and image must also change. In Carey (2009), the reflecting boundary is "pressure release," meaning that the acoustic pressure is zero on the boundary (as for the water-air interface in underwater acoustics) and the image source is equal in magnitude and *opposite* in phase to the true source.

Examining **Figure 2** further, a few critical details of the Lloyd's mirror problem emerge. Given the horizontal distance from the source to receiver (the *range*) and both the source and receiver heights, different distances are traveled by sound along the *direct* and *reflected* paths (unless the receiver is on the reflecting surface itself). This means that the received signals from the actual and image sources can differ in phase and thus reinforce or partially cancel each other. This effect is compounded if the average sound speeds along the direct and reflective paths differ as well, as occurs in real environments where the sound speed depends on parameters such as temperature and salinity that vary in time and space.

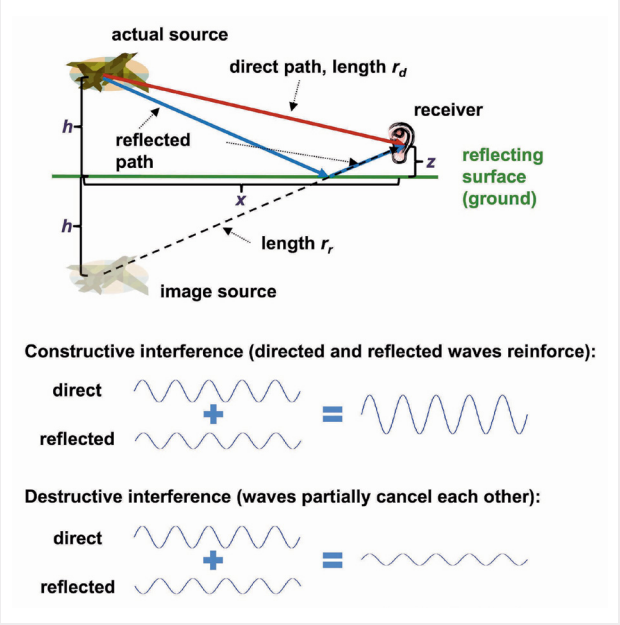

Figure 2. *Lloyd's mirror geometry and interference mechanism (**top**). **Red line:** direct path from the actual source to the receiver; **blue line:** path that reflects off the ground before reaching the receiver. The total length of the reflected path equals the length of a line drawn from an image source below the ground plane to the receiver (**dashed line**). In constructive interference (**center**), the sound along the direct and reflected paths are in phase and increase the amplitude when combined, whereas in destructive interference (**bottom**), they are out of phase, leading to decreased amplitude when combined. Here,* x *is the horizontal distance from the source to receiver,* z *is the receiver height,* r_d *is the length of the direct path (from the actual source to the receiver);* r_r *is the length of the reflected path (from the image source to the receiver); and* h *is the height of the source above the ground.*

Figure 3 shows examples of the Lloyd's mirror for propagation in air above a rigid surface, with a source height

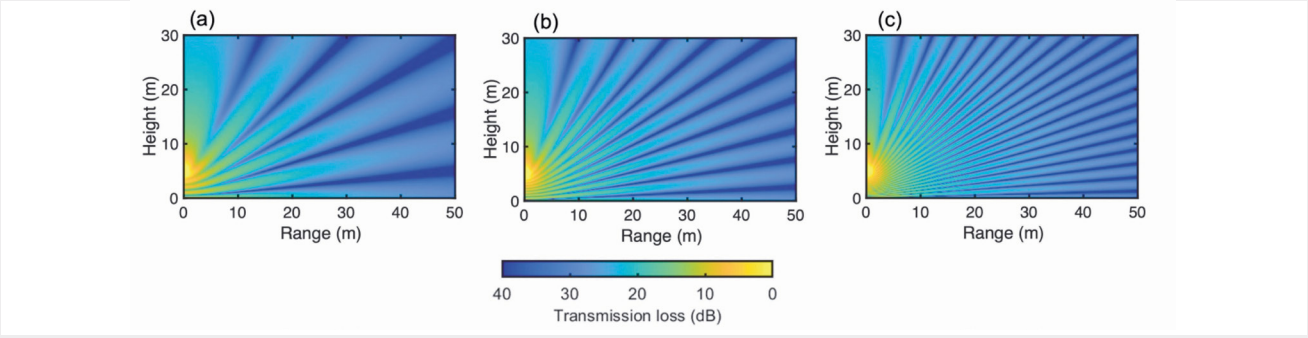

Figure 3. *Frequency dependence of the Lloyd's mirror transmission loss (TL) interference pattern.* ***a:*** *Wavelength (λ) = 2 m or 170 Hz;* ***b:*** *λ = 1 m or 340 Hz;* ***c:*** *λ = 0.5 m or 680 Hz. Darker regions indicate destructive interference (high TL), whereas lighter regions indicate constructive interference (low TL).*

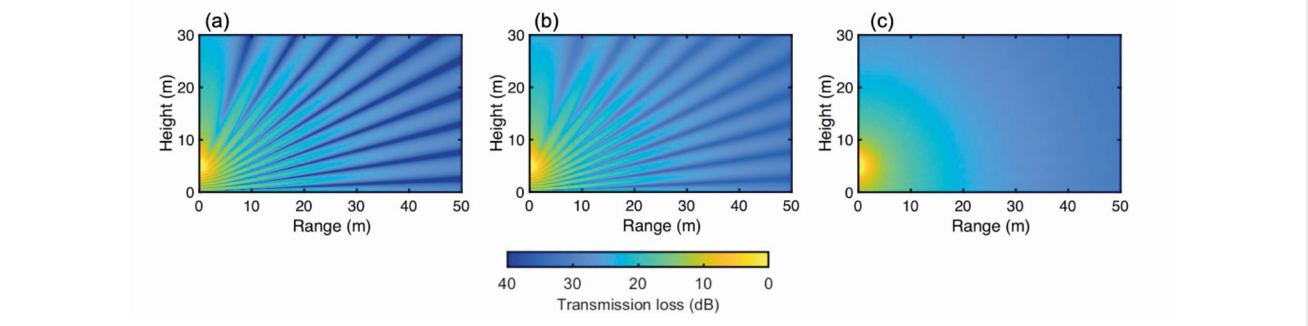

Figure 4. *Impact of uncertainties on the TL for the Lloyd mirror effect for various values of wavelength λ and variability.* ***a:*** *Small variability;* ***b:*** *medium variability;* ***c:*** *large variability. Note that increasing variability approaches the incoherent result.*

of 5 m and the same sound speed of 340 m/s along both direct and reflected paths. In **Figure 3**, we plot the transmission loss (TL), a measure of the signal loss between the source and receiver in decibels relative to the original source magnitude. TL is commonly used in propagation studies, being defined such that it equals zero at a distance of 1 m from the source in free space and increases with increasing *loss* in pressure amplitude. The frequency of the source was changed from 170 Hz (**Figure 3a**) to 340 Hz (**Figure 3b**) to 680 Hz (**Figure 3c**). These values correspond to wavelengths of 2 m, 1 m, and 0.5 m, respectively. The narrow, dark regions of **Figure 3** are receiver locations where the direct and reflected waves are very nearly out of phase with one another and thus destructively interfere. As the frequency is increased, the interferences become more closely spaced.

Impact of Uncertainty on Lloyd's Mirror

Although the mathematical description of the Lloyd's mirror effect is simple, the interference pattern can be difficult to predict accurately because it is extremely sensitive to the exact values of the model parameters. Thus, we would like to know how uncertainty in the model parameters influences the accuracy of sound field predictions.

In most practical experiments, both epistemic and aleatory uncertainties arise. Epistemic uncertainty is exemplified by not exactly knowing the range between the source and receiver or their heights. Random variations in the sound speeds, as occur from wind turbulence in the atmosphere or fluid mixing and other disturbances in a harbor, exemplify aleatory uncertainty.

Taking a probabilistic perspective, we wish to predict statistics of the sound field, in particular, the mean TL of the Lloyd's mirror problem in the presence of these uncertainties. We assume that there are five uncertain parameters: the receiver range and height, the source height, and the sound speed of the air along the direct and reflected paths.

Figure 4 plots the mean TL for three cases of increasing variability of the uncertain quantities. **Figure 4a** includes the least uncertainty and **Figure 4c** includes the most. The exact details of how the variability is specified is described later in the article, but first compare the results in **Figure 4** with those in **Figure 3b**. **Figure 3b** is the same case as **Figure 4** but assumes all model parameters are known; it is the *deterministic* result. Observe that as the amount of variability increases, the Lloyd's mirror interference pattern gradually vanishes. In fact, for the largest variability case (**Figure 4c**), the phases of the direct and reflected paths are nearly completely randomized relative to one another such that the pattern of constructive and destructive interference is averaged out. Therefore, the sound field is found simply by adding the direct and reflected energies together, in which case the two contributions are said to be *incoherent*. In ocean acoustics, coherence is diminished by scattering from ocean surface waves and bubbles (Cron and Sherman, 1962; Kuperman and Ingenito, 1980). In the atmosphere, coherence loss can be caused by turbulence (Daigle, 1979; Clifford and Lataitis, 1983). The important takeaway is that the details of the interference pattern depend on the uncertain parameters, and, therefore, the mean TL cannot be accurately predicted when these parameters are assumed to have exact, fixed values.

To further illustrate the impact of uncertainty on the interference pattern, **Figure 5** shows the TL computed at three sampled values of the sound speed from the high-variability probability density function (PDF). In **Figure 5,** *left,* the image corresponds to a sound speed of 335 m/s and the TL is between 20 and 25 dB all the way out to a 50-m range. In **Figure 5,** *center*, the image (340 m/s) has a region of high TL (a null) near the ground at a range between about 15 and 30 m. The near ground TL is important in noise applications. The image in **Figure 5,** *right* (345 m/s), has two smaller null regions near the ground. If the sound speed measurement has just a 1% error, the near-ground TL prediction at a range of 50 m could be off by as much as 15 dB!

Details of the Lloyd's Mirror Study

Probabilistic modeling requires deciding how to represent the unknown parameters with probability distributions. This is not a simple matter and very often assumptions must be made. These decisions are best informed by data, but in the absence of data, it is common to rely on expert opinions. A typical approach is to assume unknown parameters follow a *normal (Gaussian) distribution*; this simplifies the math for analytical calculations and is valid for measurements where the observed uncertainty is due to many independent, underlying random quantities. However, normal distributions are not appropriate for all situations and may, in fact, have undesirable features that preclude their use. Normally distributed random variables can take on both positive and negative values. Negative values are unlikely but still occur if the mean is positive

Figure 5. *Three evaluations of the TL for the Lloyd's mirror problem for different reflected wave sound speed: 335, 340, and 345 m/s, respectively. These sample points are also shown in relation to the probability density function (PDF) of the reflected sound speed random variable for the large variability case.* ***Colored lines and borders*** *indicate which input corresponds to which output.*

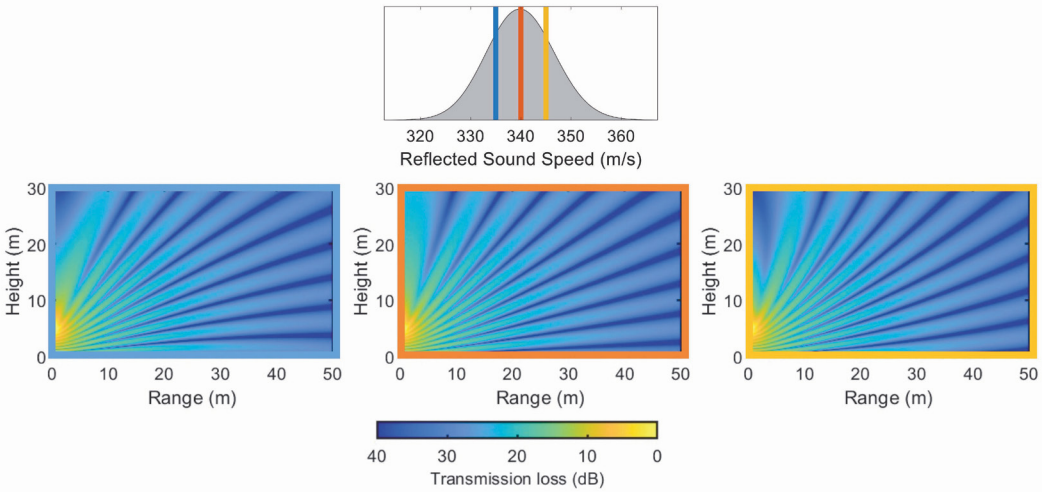

Table 1. *Mean and normalized standard deviations for the log-normal distributions, used in the cases involving small, medium, and large uncertainty*

Variability parameters used in Figures 4-6				
		Normalized standard deviation		
Variable	**Mean**	**Small**	**Medium**	**Large**
Direct sound speed	340 m/s	2×10^{-4}	2×10^{-3}	2×10^{-2}
Reflected sound speed	340 m/s	2×10^{-4}	2×10^{-3}	2×10^{-2}
Source height	5 m	1×10^{-3}	1×10^{-2}	1×10^{-1}
Receiver height	0-30 m	1×10^{-3}	1×10^{-2}	1×10^{-1}
Receiver range	0-50 m	1×10^{-3}	1×10^{-2}	1×10^{-1}

and the standard deviation is small. In the Lloyd's mirror example considered here, the uncertain parameters are all strictly positive quantities. If their assumed distributions do not share this property, negative values may lead to nonphysical results if not failure of the computer program.

The *log-normal* distribution is thus used for the Lloyd's mirror problem. This means that the *logarithms* of the parameters are normally distributed so that the parameters have the "strictly positive" property. If the mean is sufficiently large compared with the standard deviation, a log-normal distribution may appear to be very nearly the same as a normal distribution as observed in **Figure 5,** *inset*, that shows the PDF of the sound speed of the reflected path.

For the results shown in **Figure 4**, the mean (m) and normalized standard deviation (σ/m) (where σ is the usual standard deviation) for the log-normal distributions of each random variable corresponding to three different levels of variability are shown in **Table 1**. Because the source height and receiver location are uncertain, **Figure 4** was produced with the means of the receiver range and height corresponding to the position on the plot. The smaller standard deviation is used for the sound speed because the interference pattern is especially sensitive to variations in those parameters because they impact the signals' phases.

Methods for Quantifying Uncertainty in Computational Models

Two families of uncertainty quantification techniques are considered in this article to explore the impacts of uncertainty on the Lloyd's mirror effect. Both are nonintrusive. Each has a number of variants that are beyond the scope of this article. However, the following discussion provides the reader with a starting point for further investigation.

Monte Carlo Methods

Monte Carlo methods are attributed to Metropolis and Ulam (1949), who solved equations describing nuclear fission on a post-World War II computer using stacks of punch cards for input and output! They demonstrated that random sampling led to plausible results for as of then unobtainable solutions to a stochastic problem. MCS methods are well-known and used substantially in engineering studies.

MCS arose from the observation that an integral of a function of a single variable can be viewed as the probabilistic mean of the function when its argument is interpreted as a uniformly distributed random variable Thus, the integral may be computed by drawing samples from a uniform distribution, evaluating the function at those values, and calculating the sample average of the results. This approach is easily extended to multiple dimensions and straightforward to implement nonintrusively on existing codes for computing acoustic pressure fields. The primary drawback of ordinary MCS is that an impractically large number of samples are required for convergence in regions of low probability that can be important in applications where extreme values (e.g., threshold crossings) are of interest.

The errors for MCS theoretically decrease in proportion to $1/\sqrt{N}$ (Caflisch, 1998). This is slow! For the Lloyd's mirror example, using a strategy called Latin hypercube sampling (LHS), the observed rate appears closer to $1/N$, a significant speedup. If the goal is to approximately calculate the mean of the QoI (in this case TL) to within some percentage of the actual mean, and MCS achieves this with 10,000 computations of the TL, LHS can achieve the same accuracy using only 100 computations. LHS is designed to distribute the samples more evenly over the parameters than basic MCS, in which samples tend to cluster. The idea underlying LHS is to partition the domain for each random variable into N equally likely intervals, then to sample each interval just once. The order in which the intervals are sampled is random.

Generalized Polynomial Chaos

Generalized polynomial chaos (GPC) is an extension of *polynomial chaos* (PC), originally devised by Wiener (1938). PC specifically applies to expansions in terms of normal random variables, whereas Xiu and Karniadakis (2002) extended the method to accommodate a much a larger set of probability distributions, including the log-normal distributions used here. GPC involves computing the coefficients of a polynomial expansion, which turn out to be expectations of functions of the random parameters. Although the full details are beyond the scope of the present article, GPC can be approached either intrusively through derivation of a new system of equations and hence a new computer program to solve it or nonintrusively by computing the expectation integrals directly using quadrature or regression methods.

Under the right circumstances, GPC will exhibit spectral convergence (approximation error decreases exponentially fast as the number of samples is increased) and thus can solve problems with far fewer samples than MCS. For the example discussed in ***Monte Carlo Methods***, where 10,000 samples produce TL statistics accurate enough for the purpose at hand and 100 samples give the same accuracy if LHS is used, then GPC may achieve the required accuracy with only 5 samples!

GPC is also not restricted to the estimation of statistical information; the coefficients, when combined with the polynomial basis expansion, yield a surrogate (or meta-) model, which can be evaluated rapidly. The surrogate provides a polynomial representation of the complicated physics in the original computational model, which can be useful for generating realizations in a larger simulation. For example, instead of integrating a Lloyd's mirror solver into a model of aircraft noise near the ground, a GPC surrogate could be used to speed the computation. The surrogate can support design decisions by rapidly assessing which parameters are the most important. Interested readers can find further information on GPC in Wixom et al. (2019).

Figure 6 shows the relative performance of three methods for the three levels of variability. Performance is measured by how well each method predicts the mean TL shown in **Figure 4** for a given number of input samples. The error in mean TL is spatially averaged over all considered ranges and receiver heights to compute a scalar error metric for plotting in **Figure 6**. The *solid lines* in **Figure 6** show theoretical convergence rates for reference. Such an "error-per-sample-point" metric is a common measure of performance for uncertainty quantification techniques. It is often the case that the underlying deterministic model (black box) takes a long time to evaluate. Thus, a method requiring fewer samples obtains probabilistic information on the QoI much faster. Observe that MCS results track well with its theoretical convergence rate. GPC outperforms MCS and LHS for small and medium variability, but MCS and LHS perform better for large variability.

Summary

Computational models are as ubiquitous in acoustics as they are in other areas of physics. In fact, computational modeling is rapidly expanding from acoustical applications where it has been common for decades, such as underwater and structural acoustics, to others such as biological acoustics and noise. Yet trust in these models relies on systematic and rigorous assessment, which is often challenging in itself. Neglecting uncertainty can lead to misinterpretation of model results, particularly when comparing against experiments. Experimentalists have learned to characterize measurement uncertainties, but for computational acousti-

Figure 6. *Comparison of performance of different uncertainty quantification methods using dependence of the spatially averaged error in mean TL of the predictions on the number of model samples used to estimate the TL.* ***Dotted lines:*** *ordinary Monte Carlo simulation (MCS);* ***dashed lines:*** *Latin hypercube sampling (LHS);* ***dash-dot lines with diamonds;*** *generalized polynomial chaos (GPC).* ***Red lines:*** *small uncertainty case;* ***blue lines:*** *medium uncertainty;* ***green lines:*** *large uncertainty;* ***black lines:*** *reference lines for* $1/\mathrm{N}$, $1/\sqrt{\mathrm{N}}$, *and* e^{-N} *convergence rates. The reference for error was a 16,384 sample LHS result.*

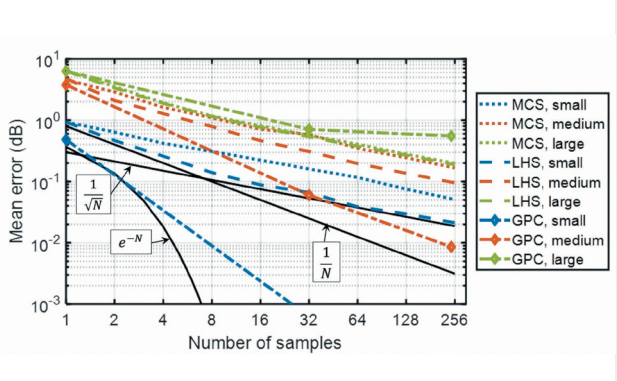

cians, this is often new territory. Nevertheless, characterizing uncertainties is a key aspect of the error budget for a given modeling effort.

We have used the Lloyd's mirror effect to demonstrate the impacts of varying degrees of uncertainty. Two popular techniques for propagating uncertainties from model input to predictions of QoI were described. It is important to note that these techniques are not "one size fits all"; the best approach is very much problem dependent.

Although we have only skimmed the topics of error analysis and uncertainty quantification in computational models, we hope the reader takes away their importance and is motivated to try incorporating the techniques presented here into their own analyses.

Acknowledgments

We are grateful for the contributions of our collaborators on some of the referenced articles. We also thank Charles Holland for insightful discussions on seabed acoustics and uncertainty.

References

Caflisch, R. (1998). Monte Carlo and quasi-Monte Carlo methods. *Acta Numerica* 7, 1-49. https://doi.org/10.1017/S0962492900002804.

Carey, W. M. (2009). Lloyd's mirror — Image interference effects. *Acoustics Today* 5, 14-20. https://doi.org/10.1121/1.3182842.

Clifford, S. F., and Lataitis, R. J. (1983). Turbulence effects on acoustic wave propagation over a smooth surface. *The Journal of the Acoustical Society of America* 73, 1545-1550. https://doi.org/10.1121/1.389416.

Cron, B. F., and Sherman, C. H. (1962). Spatial-correlation functions for various noise models. *The Journal of the Acoustical Society of America* 34, 1732-1736. https://doi.org/10.1121/1.1909110.

Daigle, G. A. (1979). Effects of atmospheric turbulence on the interference of sound waves above a finite impedance boundary. *The Journal of the Acoustical Society of America* 65, 45-49. https://doi.org/10.1121/1.382265.

Kuperman, W. A., and Ingenito, F. (1980). Spatial correlation of surface generated noise in a stratified ocean. *The Journal of the Acoustical Society of America* 67, 1988–1996. https://doi.org/10.1121/1.384439.

Metropolis, N., and Ulam, S. (1949). The Monte Carlo method. *Journal of the American Statistical Association* 44(247), 335-341. https://doi.org/10.1080/01621459.1949.10483310.

Pettit, C. L., and Wilson, D. K. (2017). Computational simulations of near-ground sound propagation. In Sarkar, S., and Witteveen, J. A. S. (Eds.), *Uncertainty Quantification in Computational Science: Theory and Application in Fluids and Structural Mechanics*, World Scientific, Singapore, pp. 33-62. https://doi.org/10.1142/9789814730587_0002.

Smith, R. C. (2013). *Uncertainty Quantification: Theory, Implementation, and Applications.* Society for Industrial and Applied Mathematics, Philadelphia, PA.

von Neumann, J. (1947), The mathematician. In Haywood, R. B. (Ed.), *Works of the Mind*. University of Chicago Press, Chicago, IL., pp. 180-196; republished in 1995 by Bródy, F., and Vámos, T. (Eds.), *The Neumann Compendium*. World Scientific, Singapore, pp. 618-626.

Wiener, N. (1938). The homogeneous chaos. *American Journal of Mathematics* 60(4), 897-936. https://doi.org/10.2307/2371268.

Wixom, A. S., Walters, G. S., Martinelli, S. L., and Williams, D. M. (2019). Generalized polynomial chaos with optimized quadrature applied to a turbulent boundary layer forced plate. *Journal of Computational and Nonlinear Dynamics* 14(2), 021010. https://doi.org/10.1115/1.4041772.

Xiu, D., and Karniadakis, G. (2002). The Wiener-Askey polynomial chaos for stochastic differential equations. *SIAM Journal on Scientific Computing* 24(2), 619-644. https://doi.org/10.1137/S1064827501387826.

Contact Information

Sheri L. Martinelli slm77@psu.edu

Undersea Systems Office
The Pennsylvania State University
State College,
Pennsylvania 16804, USA

D. Keith Wilson
d.keith.wilson@usace.army.mil

United States Army Engineer Research and Development Center
Hanover, New Hampshire 03755, USA

Andrew S. Wixom
axw274@psu.edu

Fluid Dynamics and Acoustics Office
The Pennsylvania State University
State College,
Pennsylvania 16804, USA

Chris L. Pettit pettitcl@usna.edu

Aerospace Engineering Department
United States Naval Academy
Annapolis, Maryland 21402, USA

For author bios, please go to acousticstoday.org/bios-19-2-3